ChemComm

Aqueous transfer of colloidal metal oxide nanocrystals via base-driven ligand exchange

Journal:	*ChemComm*
Manuscript ID	CC-COM-04-2022-002416.R1
Article Type:	Communication

COMMUNICATION

Aqueous transfer of colloidal metal oxide nanocrystals *via* base-driven ligand exchange

Received 00th January 20xx,
Accepted 00th January 20xx

DOI: 10.1039/x0xx00000x

Vikram S. Lakhanpal,[a] Benjamin Z. Zydlewski,[b] Xing Yee Gan,[a] Hugo Celio,[c] Huei-Ru "Molly" Jhong,[a] Charles K. Ofosu,[b] Delia J. Milliron*[a]

A general method is developed for removal of native nonpolar oleate ligands from colloidal metal oxide nanocrystals of varying morphologies and compositions. Ligand stripping occurs by phase transfer into potassium hydroxide solution, yielding stable aqueous dispersions with little nanocrystal aggregation and without significant changes to the nanomaterials' physical or chemical properties. This method enables facile fabrication of conductive films of ligand-free nanocrystals.

Colloidal nanocrystal (NC) synthesis is a well-established method for creating nanomaterials with good morphological control and long-term stability[1,2]. These advantages are due in part to the use of surface-passivating ligands, typically long-chain hydrocarbons such as oleylamine and oleic acid. However, many applications of these materials, including catalysis, electrochemical devices, and charge transport, require removal of these bulky, insulating ligands to access the material's unique surface properties[3–5]. One approach is to replace them with shorter, inorganic ligands, which can enhance charge transport between NCs or enable gelation into porous catalytic materials[6–8]. Another method uses Meerwein's salt or its derivatives to cleave the ligand-NC bond and stabilize NCs with weakly interacting tetrafluoroborate or hexafluorophoshate anions in solution[9–12]. These processes yield dispersions in polar organic solvents such as dimethylformamide; however, transfer to aqueous dispersions would offer distinct advantages in processing out of a non-toxic solvent, compatibility with certain polymers, and biological applications[13–15].

Aqueous dispersions of NCs are usually obtained by replacing native hydrophobic ligands with hydrophilic ligands or polymers. For example, polyoxometalate (POM) ligands offer stability in water and can lead to unique phase transformations after film casting[16,17]. Another method functionalized NCs with a hydrophilic copolymer before aqueous transfer with a buffer solution[18], and was later used to make tin-doped indium oxide (ITO) NC dispersions used for spraycoating electrochromic devices and biosensing in bacterial environments[19,20]. However, Jhong and coworkers obtained an aqueous dispersion of ITO NCs without any surface-adsorbed polymer using a two-phase transfer into a highly basic potassium hydroxide (KOH) solution followed by spin dialysis purification. The resulting hydroxyl-functionalized NCs had chemically accessible surfaces, allowing them to act as electrocatalysts for the selective reduction of CO_2 to formate[21]. Considering the cost and environmental benefits of aqueous processing and the need to avoid bulky, insulating coatings for many applications, there is great motivation to generalize this success to other metal oxide NC compositions.

In this work, we expand on this base-driven method to cover several metal oxide NCs of varying compositions, shapes, and sizes. We begin with cerium-doped indium oxide (CIO), a promising material for transparent conducting coatings[22], and achieve successful aqueous transfer that results in a stable, ligand-free dispersion. Further characterization *via* transmission Fourier-transform infrared spectroscopy (FTIR), X-ray photoelectron spectroscopy (XPS) and X-ray diffraction (XRD) indicates the oleate ligands are replaced with hydroxyl groups and the exchange process has no detectable changes to the crystal structure or morphology of the NCs. However, XPS also shows the base stripping process oxidizes the cerium dopant and decreases its concentration near the surface. We adapt the method for four additional metal oxide NC compositions. Finally, we spincoat an aqueous dispersion of ITO NCs to produce a transparent conducting film, demonstrating the stripping process's utility to generate functional materials.

The base-stripping process involves phase transfer of NCs from hexane to alkaline water. For example, as-synthesized, oleate-capped CIO NCs (CIO-C, 5% Ce doping) dispersed in hexane (2.5 mg/mL) were placed in a vial over an aqueous solution of 0.2 M KOH and stirred for 24 hours. The hexane

[a] *McKetta Department of Chemical Engineering, University of Texas at Austin, Austin, Texas 78712, United States.*
[b] *Department of Chemistry, University of Texas at Austin, Austin, Texas 78712, United States.*
[c] *Texas Materials Institute and Materials Science and Engineering Program, The University of Texas at Austin, Austin, TX 78712, United States.*
Electronic Supplementary Information (ESI) available: [details of any supplementary information available should be included here]. See DOI: 10.1039/x0xx00000x

phase was removed and the aqueous phase diluted and purified *via* spin dialysis. A full account of experimental methods and characterization is included in the Supporting Information.

After stripping, the NCs (CIO-S) retain their rounded cubic shape with a slight increase in average size from 18.8 ± 3.5 nm to 19.4 ± 3.5 nm, as shown by bright-field scanning transmission electron microscopy (BF-STEM) (Figure 1a). FTIR of CIO-C and CIO-S dropcast onto silicon reveals a reduced intensity of C-H stretching peaks between 2800 and 3000 cm^{-1} in CIO-S, confirming the successful removal of oleate ligands (Figure 1b). Additionally, a shift in the localized surface plasmon resonance (LSPR) peak frequency, from 2150 cm^{-1} to 2041 cm^{-1}, may reflect slightly stronger LSPR coupling between neighboring NCs[23]. The zeta potential shifts from 2.2 mV to -53.7 mV after stripping (Figure 1c). This indicates that as-synthesized NCs form a sterically stabilized colloidal dispersion in non-polar solvents like hexane, while base-stripped NCs are stabilized in water by strong electrostatic repulsion between their negatively charged surfaces[19,21]. Dynamic light scattering (DLS) of dilute samples of CIO-C and CIO-S shows an increase in hydrodynamic diameter from 28.2 nm to 43.8 nm, suggesting the stripped particles have slight aggregation (Figure 1d).

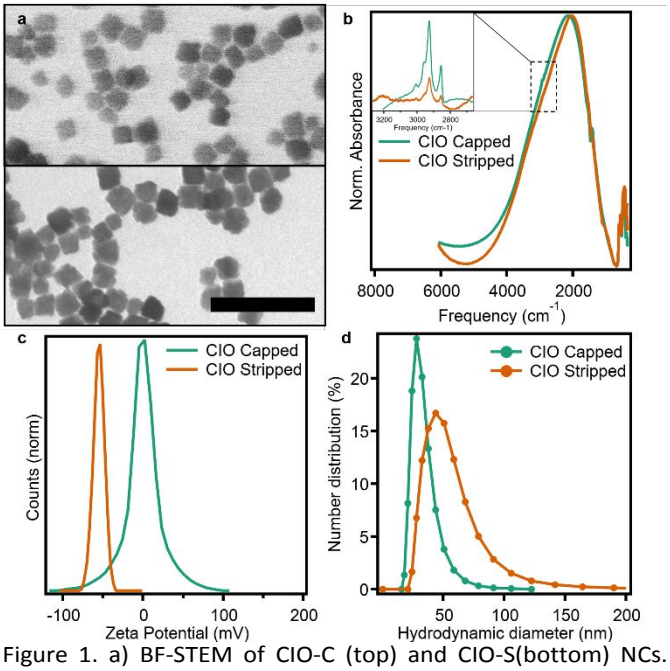

Figure 1. a) BF-STEM of CIO-C (top) and CIO-S(bottom) NCs. Scale bar is 100 nm. b) FTIR spectra of CIO-C and CIO-S normalized to LSPR peak, with C-H stretch region highlighted (inset). c) Zeta potential and d) DLS of CIO-C and CIO-S.

The overall crystal structure is unaffected by the stripping process; XRD patterns show the characteristic bixbyite structure peaks appear in the same positions for capped and stripped CIO NCs (Figure S3). A closer examination of the (222) peak observed at 30.5° shows a slight shift to lower 2θ after stripping, suggesting a similarly slight increase in the lattice parameter. Scherrer analysis of the broadened peak indicates a slight decrease in average crystallite size from 17.7 nm to 15.2 nm.

To further examine the effect of the ligand stripping process on the composition and structure of the NCs, XPS were taken of O 1s (Figure 2), In 3d, and Ce 3d (Figure S4) orbitals. The O 1s spectra feature a prominent peak at approximately 529.8 eV with a sizable shoulder at higher binding energy. While the peak can be readily assigned to oxygen in the NC lattice, interpreting the nature of oxygen in the shoulder is more complicated, with several possible species to which it could be assigned. Given the ligands involved in the stripping reaction, we assigned two peaks to carboxylate (532.4 eV) and hydroxyl (531.5) groups bound to the NC surface. A fourth, intermediate peak for defect-adjacent oxygen (DAO) was added at 530.5 eV. This peak is attributed to oxygen in the lattice that is not fully coordinated due to proximity to the surface, an oxygen vacancy, or some other defect in the lattice[24,25]. To quantitatively analyze the results, the areas of each peak are normalized to the total area of the In 3d peaks in their respective samples (Table S1). The lattice oxygen and DAO peaks show practically no change in area and have a slight shift (~0.1 eV) to lower energy. Combined with the XRD results, this result indicates the stripping process did not substantially affect the NC structure. At higher binding energies, the hydroxyl peak grows slightly after stripping, while the carboxylate peak is diminished.

The In 3d spectra appear unaffected by the ligand stripping, with no appreciable shift in the peak positions or shapes. However, prominent changes are observed in the Ce 3d spectra. While the capped sample is fit to peaks associated with Ce^{3+}, a characteristic Ce^{4+} peak emerges in the stripped sample, and we calculate that 20% of Ce ions are 4+. (Full analysis is included in the SI.) The prevalence of Ce near the NC surface decreases from 3.86% to 3.15% relative to the total metal ion content. The XPS data thus suggest hydroxyls react preferentially with cerium ions near the NC surface, causing selective leaching of cerium and partial oxidation of the remaining near-surface ions. To support this, we performed inductively coupled plasma optical emission spectroscopy (ICP-OES) to see if the overall doping amount decreased. The overall Ce dopant percentage was 2.63 ± 0.10% for CIO-C and 2.82 ± 0.04% for CIO-S. Since the overall doping amount does not decrease, it only changes near the surface, confirming selective leaching by the base.

Upon successfully developing a ligand stripping procedure for CIO NCs resulting in a stable aqueous dispersion with little aggregation and no significant physical changes to the NCs, we sought to generalize this method to other NC compositions. With little variation, we successfully adapted this procedure for ~22 nm undoped indium oxide (UIO) spheres and ~15 nm ITO (8% Sn doping) spheres, smaller than the 20 nm ITO NCs used by Jhong *et al*[21]. Like CIO, UIO and ITO NCs were synthesized by a slow injection method and were similarly capped with oleic acid. During ligand exchange, the transfer time into the aqueous phase for UIO NCs was the same (24 hours) as for CIO NCs, while ITO NCs took slightly longer (28 hours) to fully transfer. We also stripped smaller (8.4 nm) titanium oxide (TiO_2) platelets, synthesized with a hot injection method. The platelets were also functionalized with oleic acid, but required 40 hours to fully transfer into water. Despite the differences in composition and morphology, all four oleate-capped NCs were stripped with the same method, save for a change in stripping time. Additionally, this trend between NC size and stripping time is consistent with the idea that larger NCs have faster ligand exchange kinetics due

to greater surface area and lower ligand density[26]. Compared to the larger NCs, 4.5 nm cerium oxide (CeO_2) spheres required significant changes to the procedure. KOH concentration was increased to 1 M, while the initial NC concentration in hexane was lowered to 1 mg/mL to ensure successful base stripping. While this synthesis used oleylamine as the NC ligand, a recent study reports that oleylamine is converted to oleate when used with a nitrate precursor in NC syntheses similar to our CeO_2 synthesis[27]. Thus, it is probable that the CeO_2 NCs are oleate capped, and we conclude smaller NCs require more aggressive base stripping, either by longer stripping time or increased pH.

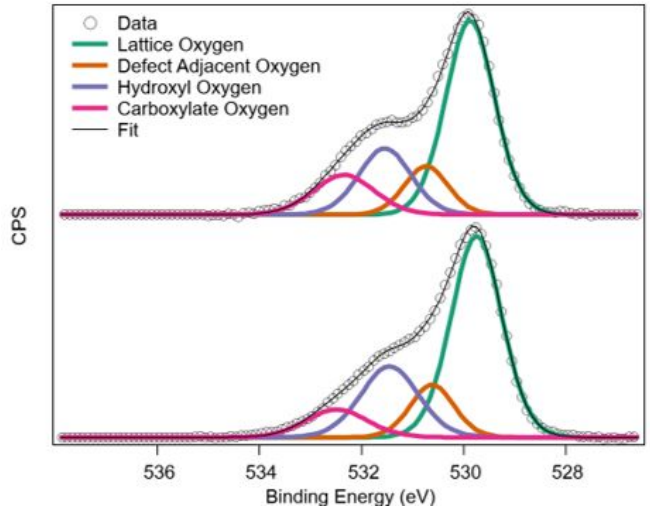

Figure 2. XPS of O 1s spectra and their fitted peaks for CIO-C (top) and CIO-S (bottom).

All of these materials underwent the same characterization as CIO before and after stripping. Key parameters obtained from BF-STEM, DLS, and zeta potential are listed in Table 1; corresponding images and plots are included in the supporting information, as are FTIR, XRD, and XPS data (Figures S5-S16). Quantitative analysis of oxygen and metal XPS spectra are listed in Table S2. In general, NC size was unaffected; while the average diameter of UIO by BF-STEM increased 6.8% after stripping, the magnitude of size change in the other samples were all between 3 and 4.5%. The slight increases observed in average particle size can be attributed to the loss of some smaller particles due to incomplete stripping. Each material also exhibited a small increase in hydrodynamic diameter and a shift to highly negative zeta potentials. The NC shapes remained fairly constant before and after stripping for each material, as did the crystal structures. All materials showed similar behavior as the CIO NCs before and after ligand stripping. XPS of ITO showed a decrease in near-surface Sn content after stripping, from 7.02% to 6.31%, similar to the decrease in surface Ce doping in CIO. ICP-OES of ITO showed a decrease in overall Sn doping from 6.66 ± 0.10% to 6.17 ±0.08%. This decrease is smaller than the drop near the surface per XPS, again indicating a selective leaching of Sn during the stripping. Analysis of the Ce 3d spectra in CeO_2 determined the relative amounts of cerium's oxidation states; the Ce^{4+} content increases from 64% to 87%, showing how the base oxidizes these ions near the NC surface. Dispersion spectra of CIO and ITO show a decrease in LSPR extinction after stripping accompanied by asymmetric peak broadening. This suggests a decrease in carrier concentration in both materials. The band edges for both materials show slight shifts to lower energy, consistent with mid-gap electronic states forming due to increased hydroxylation[28] (Figures S17-18).

To demonstrate the utility of the base-stripping method, we fabricated NC films spincoated from aqueous ITO-S dispersions. These films are of similar thickness and show similar random NC arrangement (Figures S19-20). We measured conductivity of the films at room temperature using a four-point Van der Pauw configuration. The resistivity of the ITO-S film is 4.1 Ω-m, nearly 5 times less resistive than the ITO-C film's resistivity of 19.5 Ω-m (Figure 3a). From this we conclude the aqueous transfer of ligand stripped ITO NCs enables closer packing in spincoated films with easier electron transfer between them. The ITO-S film displays greater transparency than the ITO-C film in the visible spectrum but has lower transmittance across much of the near-infrared region (Figure 3b). As such, the integrated solar transmittance is similar between the two samples: 82% for the ITO-C film and 85% for the ITO-S film. The ITO-S film is more hydrophilic, with smaller contact angles than the ITO-C film, and has a greater surface energy (Table S3-4). In sum, we were able to fabricate thin films out of aqueous, ligand-stripped ITO NCs with improved conductivity over capped NC films that maintain similar solar transmittance. This allows us to avoid toxic organic solvents for deposition as well as further ligand removal treatments. This ease of improved fabrication can extend to other studies of NC thin films or preparation of NC-based catalysts with accessible surfaces.

Sample	Shape	d_{core} (nm)	d_H (nm)	ζ (mV)
In_2O_3-C	Sphere	21.9 ± 3.0	37.8	8.8
In_2O_3-S	Sphere	23.4 ± 2.6	50.8	-50.9
Ce:In_2O_3-C	Cube	18.8 ± 3.5	28.2	2.2
Ce:In_2O_3-S	Cube	19.4 ± 3.5	43.8	-53.7
Sn:In_2O_3-C	Sphere	14.8 ± 1.6	18.2	4.2
Sn:In_2O_3-S	Sphere	14.3 ± 1.3	35.3	-44.4
CeO_2-C	Sphere	4.5 ± 0.9	15.7	-0.5
CeO_2-S	Sphere	4.3 ± 0.7	18.2	-31.9
TiO_2-C	Plate	8.4 ± 1.4	21.0	3.8
TiO_2-S	Plate	8.7 ± 1.5	50.8	-37.3

Table 1. Particle shape, size (*via* BF-STEM), hydrodynamic diameter (*via* DLS), and zeta potential for each material before (-C) and after (-S) ligand stripping.

In conclusion, we developed a ligand removal process using concentrated KOH solution for a variety of metal oxide NCs. This yielded stable aqueous NC dispersions, from which we could spincoat films to take advantage of the material's unique surface properties. While only minor changes were observed in the surface chemical composition and chemical environments by XPS, further studies of composition *via* Raman and UV-visible spectroscopy may reveal changes in the concentration and

distribution of oxygen vacancy defects[25,28,29]. Considering the role surface structure plays in NC optoelectronic properties and catalytic activity, such studies may be carried out in concert with investigations of specific functional properties[30–32]. It is also worth investigating if this method can be adapted to different NC shapes or ligand cappings. While we demonstrate this method on many metal oxide NCs, it is important to note that further generalization must account for a material's stability in basic conditions. For example, we found that cesium-doped tungsten oxide NCs dissolve at high pH, rendering this method impractical for that system. Nonetheless, this development broadens options for processing of colloidally grown NCs and enables use of water for environmentally friendly processing, creating exciting new opportunities for their application.

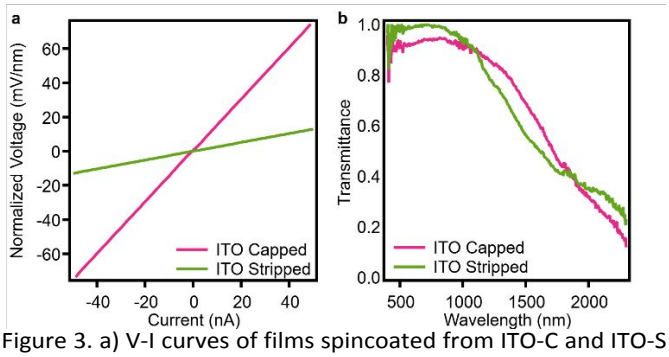

Figure 3. a) V-I curves of films spincoated from ITO-C and ITO-S dispersions. ITO NCs are 14.8 nm with 8% Sn doping. Voltages are normalized to film thickness so slopes represent resistivity. b) Optical transmittance of ITO-C and ITO-S spincoated films in visible and near-infrared light backgrounded to glass reference.

V.S.L., D.J.M. initiated and designed studies. V.S.L., B.Z.Z., H.C. collected and analysed data. V.S.L., M.J., X.Y.G. developed methodology. B.Z.Z., H.C., C.K.O. provided resources. V.S.L. prepared data visualization and wrote original draft, revised by B.Z.Z., H.C., X.Y.G., D.J.M. D.J.M. supervised the project.

This work was supported by an Air Force STTR Grant (#UTA20-000531) (V.S.L., D.J.M.), a CBBM grant (#UTA16-000941) (B.Z.Z., D.J.M.), the Welch Foundation (F-1848), and the National Science Foundation through the Center for Dynamics and Control of Materials: an NSF MRSEC (Grant# 1720595) (X.Y.G., C.K.O.). V.S.L. would also like to thank Gary K. Ong for synthesis of the TiO_2 NCs used in this study.

There are no conflicts to declare.

References

1 R. Buonsanti, D. J. Milliron, *Chem. Mater.*, 2013, **25**, 1305-1317.
2 W. Wang, M. Zhang, Z. Pan, G. M. Biesold, S. Liang, H. Rao, Z. Lin, X. Zhong, *Chem. Rev.*, 2022, **122**, 4091-4162.
3 J. Huang, R. Buonsanti, *Chem. Mater.* 2019, **31**, 13-25.
4 S. Heo, J. Kim, G. K. Ong, D. J. Milliron, *Nano Lett.*, 2017, **17**, 5756-5761.
5 E. L. Runnerstrom, G. K. Ong, G. Gregori, J. Maier, D. J. Milliron, *J. Phys. Chem C*, 2018, **122**, 13624-13635.
6 A. Nag, M. V. Kovalenko, J.-S. Lee, W. Liu, B. Spokoyny, D. Talapin, *J. Am. Chem. Soc.*, 2011, **133**, 10612-10620.
7 A. Levi, L. Verbitsky, N. Waiskopf, U. Banin, *ACS Appl. Mater. Interfaces*, 2022, **14**, 647-653.
8 G. Jiang, J. Want, N. Li, R. Hübner, M. Georgi, B. Cai, Z. Li, V. Lesnyak, N. Gaponik, A. Eychmüller, *Chem. Mater.*, 2022, **34**, 2687-2695.
9 A. Dong, X. Ye, J. Chen, Y. Kang, T. Gordon, J. M. Kikkawa. C. Murray, *J. Am. Chem. Soc.*, 2011, **133**, 998-1006.
10 M. A. Caldwell, A. E. Albers, S. C. Levy, T. E. Pick, B. E. Cohen, B.A. Helms, D.J. Milliron, *Chem Commun.*, 2011, **47**, 556-558.
11 E. L. Rosen, R. Buonsanti, A. Llordes, A. M. Sawvel, D. J. Milliron, B. A. Helms, *Angew. Chem. Int. Ed.*, 2012, **51**, 684-689.
12 A. Paolella, G. Bertoni, S. Marras, E. Dilena, M. Colombo, M. Prato, A. Riedinger, M. Povia, A. Ansaldo, K. Zaghib, L. Manna, C. George, *Nano Lett.*, 2014, **14**, 6828–6835.
13 D. Song, M. Li, Y. Li, X. Zhao, B. Jiant, Y. Jiang, *ACS Appl. Mater. Interfaces*, 2014, **6**, 7126-7132.
14 N. M. Nair, J. K. Pakkathilliam, K. Kumar, K. Arunachalam, D. Ray, P. Swaminathan, *ACS Appl. Electron. Mater.*, 2020, **2**, 1000-1010.
15 W. Song, S. Soo Lee, M. Savini, L. Popp, V. L. Colvin, L. Segatori, *ACS Nano*, 2014, **8**, 10328-10342.
16 A. Llordes, A. T. Hammack, R. Buonsanti, R. Tangirala, S. Aloni, B. A. Helms, D. J. Milliron, *J. Mater. Chem.*, 2011, **21**, 11631-11638.
17 J. Huang, W. Liu, D. S. Dolzhnikov, L. Protesescu, M. V. Kovalenko, B. Koo, S. Chattopadhyay, E. V. Shenchenko, D. V. Talapin, *ACS Nano*, 2014, **8**, 9388-9402.
18 J. T. Guong, M. J. Bailey, T. E. Pick, P. M. McBride, E. L. Rosen, R. Buonsanti, D. J. Milliron, B. A. Helms, *J. Polym. Sci. Part Polym. Chem.*, 2012, **50**, 3719-3727.
19 A. Maho, C. A. Saez Cabezas, K. A. Meyertons, L. C. Reimnitz, S. Sahu, B. A. Helms, D. J. Milliron, *Chem. Mater.*, 2020, **12**, 8401-8411.
20 A. J. Graham, S. L. Gibbs, C. A. Cabezas, Y. Wang, A. M. Green, D. J. Milliron, B. K. Keitz, *ChemElectroChem*, 2022, **9**.
21 H.-R. "Molly" Jhong, U. O. Nwabara, S. Shubert-Zuleta, N. S. Grundish, B. Tandon, L. C. Reimnitz, C. M. Staller, G. K. Ong, C. A. Saez Cabezas, J. B. Goodenough, P. J. A. Kenis, D. J. Milliron, *Chem. Mater.*, 2021, **33**, 7675-7685.
22 B. H. Kim, C. M. Staller, S. H. Cho, S. Heo, C. E. Garrison, J. Kim, D. J. Milliron, *ACS Nano*, 2018, **12**, 3200-3208.
23 O. Zandi, A. Agrawal, A. B. Shearer, L. C. Reimnitz, C. J. Dahlman, C. M. Staller, D. J. Milliron, *Nat. Mater.*, 2018, **17**, 710-717.
24 J.-C. Dupin, D. Gonbeau, P. Vinatier, A. Levasseur, *Phys. Chem. Chem. Phys.*, 2000, **2**, 1319-1324.
25 L. Wang, Y. Dong, T. Yan, Z. Hu, A. A. Jelle, D. M. Meira, P. N. Duchesne, J. Y. Y. Loh, C. Qiu, E. E. Storey, Y. Xu, W. Sun, M. Ghoussoub, N. P. Kherani, A. S. Helmy, G. A. Ozin, *Nat. Commun.*, 2020, **11**, 2432.
26 Y. Shen, M. Abolhasani, Y. Chen, L. Xie, L. Yang, C. W. Coley, M. G. Bawendi, K. F. Jensen, *Angew. Chem. Int. Ed.*, 2017, **56**, 16333-16337.
27 M. Calcabrini, D. Van den Eynden, S. S. Ribot, R. Pokratath, J. Llorca, J. De Roo, M. Ibáñez, *JACS Au*, 2021, **1**, 1898-1903.
28 C. Fan, C. Chen, J. Wang, X. Fu, Z. Ren, G. Qian, Z. Wang, *Sci. Rep.*, 2015, **5**, 11712.
29 A. Naldoni, M. Allieta, S. Santangelo, M. Marelli, F. Fabbri, S. Cappelli, C. L. Bianchi, R. Psaro, V. Dal Santo, *J. Am. Chem. Soc.*, 2012, **134**, 7600-7603.
30 B. Tandon, S. A. Shubert-Zuleta, D. J. Milliron, *Chem. Mater.*, 2022, **34**, 777-788.
31 M. Ghini, N. Curreli, M.B. Lodi, N. Petrini, M. Wang, M. Prato, A. Fanti, L. Manna, I. Kriegel, *Nat. Commun.*, 2022, **13**, 537.
32 T. S. Sreeremya, A. Krishnan, K. C. Remani, K. R. Patil, D. F. Brougham, S. Ghosh, *ACS Appl. Mater. Interfaces*, 2015, **7**, 8545-8555.